Annals of Nuclear Energy 115 (2018) 16–26

Contents lists available at ScienceDirect

Annals of Nuclear Energy

journal homepage: www.elsevier.com/locate/anucene

Dynamic response analysis of corrosion products activity under steady state operation and Mechanical Shim based power-maneuvering transients in *AP-1000*

Fiaz Mahmood, Huasi Hu *, Liangzhi Cao

School of Nuclear Science and Technology, Xi'an Jiaotong University, Xi'an, Shaanxi 710049, China

ARTICLE INFO

Article history:
Received 19 October 2017
Received in revised form 9 January 2018
Accepted 12 January 2018
Available online 2 February 2018

Keywords:
Corrosion products
Specific activity
Steady state operation
Power transients
AP-1000

ABSTRACT

The advanced *Mechanical Shim* (*MSHIM*) core control strategy is a flexible power-maneuvering feature of *AP-1000* reactor. This is vulnerable for variation in *Activated Corrosion Products (ACPs)* buildup while providing frequent power maneuver opportunities. It is therefore important to study the *ACPs* buildup behavior in *AP-1000* reactor. A new simulation methodology is developed to analyze the specific activity due to *ACPs* under steady state operation and *MSHIM* based power-maneuvering transients. The dynamic response of coolant specific activity due to corrosion products (^{56}Mn, ^{59}Fe, ^{24}Na, ^{60}Co and ^{99}Mo) has been analyzed under steady state full power operation. It is observed that short-lived ^{56}Mn and ^{24}Na are major sources of predominant and total coolant specific activity during reactor operation, whereas long lived *ACPs* mainly contributed after shutdown. The parametric study of *MSHIM* control based daily load follow operation, step load, load regulation and scram transients is also carried out. It is found that specific activity increases or decreases directly as a function of power maneuvering levels during daily load follow and load regulation transients. However, if power becomes constant followed by the decreasing power maneuvering, the specific activity retains its prior behavior and finally attains a lower constant value. For the step load transients, the specific activity value increases sharply and finally reaches a new saturation level. In all of the anticipated power maneuvering transients, the post saturation specific activity value shows direct relation with net change in power before and after the transients. The higher the difference between pre-transient and post-transient power levels, the longer it takes to achieve saturation value and vice versa. For postulated scram transients, it is observed that the specific activity due to ^{56}Mn suddenly decreases after the transients mainly due to its short half-life and discontinuation in further production.

1. Introduction

The water is a cost effective medium of heat transfer in nuclear reactors but it causes corrosion in materials; in contact with it. Thus, some *Corrosion Products (CPs)* are released into water, which become neutron-activated while passing through the reactor core. The *Activated Corrosion Products* (*ACPs)* create a gamma radiation field when deposited outside the reactor core, giving rise to serious radiation hazards for the inspection and maintenance teams (Comley, 1985; Lister, 1984). More than 90% of *Occupational Radiation Exposure (ORE)* is caused by *ACPs*, which leads to high post shutdown radiation levels (Li et al., 2017a). This results in prolonged maintenance schedules and lowered plant availability factor, causing loss of revenues mounting to several million dollars per plant per annum (Mirza et al., 2011). The inhibition of corrosion has been a serious industrial challenge and different methods are being practiced accordingly. Recently, the use of surfactants as corrosion inhibitors in different environments has been optimized by developing semi-empirical, mechanistic, combined semi-empirical and mechanistic, and multi-physics models. (Zhu et al., 2017).

The *Pressurized Water Reactors (PWRs)* constitute dominant majority of both operational as well as under construction nuclear power plant units in the world (IAEA, 2015). Therefore, an extended focus has been attributed to study *Corrosion Products Activity (CPA)* in *PWRs*, with main emphasize on typical operational *PWRs*. The next generation nuclear reactors are gaining economic improvements through extended cycle length, reduced plant outages and improved neutronics designs. While shifting from

* Corresponding author.
E-mail address: huasi_hu@mail.xjtu.edu.cn (H. Hu).

https://doi.org/10.1016/j.anucene.2018.01.009
0306-4549/

12-month to 18-month fuel cycle, power capacity is substantially increased by 3–7%. But with increasing operating fuel cycle duration, the amount of CRUD also increases ultimately causing enhanced *ORE* (Song and Lee, 2003). The installation of new generation *PWRs*, having modified neutronics design and extended fuel cycle length, demands more emphasized considerations to study *CPA* effect (IAEA, 2012). Therefore, it is important to analyze *CPA* behavior for all categories of *PWRs* having variable operating parameters; like fuel enrichment, burn up, stretch out length and operational transients.

The *AP-1000* is a Generation III+ (two-loop, 18 month fuel cycle) *PWR*, having passive safety features and extensive plant simplifications (Sutharshan et al., 2011). Traditional *PWRs* utilize the control rods movement associated with adjustments of the soluble boron concentration in the moderator, for power adjustments (Westinghouse Electric Company, 2005). However, the advanced *MSHIM* based control system in *AP-1000* uses solely control rods to perform the power maneuvers. It has a major advantage of maneuvering load follow without changing the soluble boron concentration in the moderator for up to 95% of cycle (Onoue and Kawanishi, 2003). The *MSHIM* based power maneuvering feature used in *AP-1000* is a flexible approach of reactor control without introducing a large perturbation in power distribution. This feature has enhanced the favorability to use *PWRs* for the frequent load follow operations to meet grid requirements and better reactor control during slow and fast transients. However, frequent power maneuvering ability has also enhanced the frequency of *CPA* variation during such transients. The *CPA* variation has direct consequences on gamma field because the concentration of gamma emitter A*CPs* is subjected to reactor operational conditions. The estimation of variation in radiation levels is a major concern regarding accessibility of coolant circuit equipment and instruments during small-scale loss of coolant incidents. Therefore, it is important to assess the impact of *MSHIM* based power maneuvering transients on dynamic behavior of *CPA* in *AP-1000*.

In the past, extensive efforts have been made to develop models for the estimation of *CPA* buildup and transport in *Light Water Reactors (LWRs)*. These models are either empirical or semi-empirical in nature, derived from either experimental data or plant design data (Rafique et al., 2010). The surface roughness is an important parameter effecting corrosion rate and ultimately the buildup behavior of *ACPs* in the *PWR* environment. Researchers have experimentally investigated the effect of surface roughness on corrosion of thermally treated *(TT)* Alloy 690 under influence of primary coolant at 330 °C (Seo et al., 2015). In the previous decades, several studies were focused on coolant activation in a typical *PWR* having constant corrosion rates and undergoing through perturbations (Deeba et al., 1999; Mirza et al., 1998). These studies have also been extended for analyzing the behavior of A*CPs* for linearly and non-linearly rising corrosion rates under flow transients in a *PWR* (Mirza et al., 2005; Rafique et al., 2003). Recently, effect of flow rate perturbations has been studied using the computer program *CPAIR-P* for time dependent corrosion rates in *PWRs* having extended cycles (Nasir et al., 2017). They observed *CPA* behavior of ^{56}Mn, ^{24}Na, ^{59}Fe, ^{98}Mo and ^{60}Co. The properties of these isotopes are shown in Table 1.

A code CTAM-II was developed to evaluate *CPA* in the primary coolant water of *Deep-Sea Reactor X (DRX)*. The *DRX* is a small *PWR* without purification system, which is designed to provide undersea power sources (Odano and Ishida, 2000). A simple mathematical model based on balance between rate of production and decay of radioactive *CPs* was established, to simulate the *ACPs* in primary coolant of a *Miniature Neutron Source Reactor (MNSR)* (Soukieh et al., 2012). An increasing trend in primary coolant activity, with ^{24}Na activity having much higher contribution as compared to ^{27}Mg, was found in the *MNSR*. The application of developed *CPA* models and computer codes valid for one reactor type to another reactor type, proved a good analysis tool to analyze *CPA* for new reactor designs. Based on the OSCAR code, mainly used for *PWRs*, a new code OSCAR-Na has been developed for contamination and mass transfer assessment in the primary circuit of *Sodium Cooled Fast Reactor (SFR)* (Génin et al., 2016). Due to similarity in thermal-hydraulic design of both *PWR* and fusion reactors, the CATE code was developed on the basis of *PWR* experiences to analyze *CPA* in International *Thermonuclear Experimental Reactor (ITER)* and *China Fusion Engineering Test Reactor (CFETR)* (Li et al., 2017a, b; Zhang et al., 2015).

The previous studies have mainly focused on typical *PWRs* but with increasing tendency of installation of new *PWR* designs, the study of *CPA* behavior in *AP-1000* also gained fame. The CAT 1.0 code was developed to study the corrosion inhabitation effects of Zn injection in the *Reactor Coolant System (RCS)* of *AP-1000* (Jia, 2016; Shuran, 2016). But previous studies were not aimed to investigate the effect of design based power transients on *CPA* in *AP-1000*. The, present study is aimed to predict the dynamic response of *CPA* in *AP-1000* during steady state operation and *MSHIM* based power-maneuvering transients. To simulate the dynamic behavior of *CPA* in the primary coolant loop of *AP-1000*, a MATLAB program *Corrosion Products Activity in AP-1000 (CPA-AP1000)* has been developed. The program is based on a well-tested kinetic model of *CPA* in typical *PWRs* (Deeba et al., 1999). The necessary neutronics calculation for *AP-1000* reactor core was performed using *MCNP* code. The *CPA* behavior has been analyzed and quantified for steady state and daily load follow operations. Moreover, the analyses have also been carried out for step load changes and load regulation transients.

The rest of paper is organized as follows: Section 2 describes the mathematical model and necessary parameters. Section 3 contains the computing scheme used to calculate the specific activity for different scenarios. Section 4 is composed of results and discussion of a variety of analyses such as sensitive parameter of the model and the *CPA* behavior under normal operation and transients. Section 5 is the conclusion of the present research along with discussion of enhancing the scope of the current work.

2. Mathematical model

The mathematical model of time dependent activity buildup resulting from the activation of corrosion products in the primary coolant loop of a typical water-cooled reactor is based on the following assumptions (Deeba et al., 1999; Jaeger, 1970)

- The material of walls of cooling system corrodes uniformly and homogeneously and composition of *CPs* corresponds to the chemical composition of originally corroding material.
- The deposition of the activity on surfaces in contact with cooling water is proportional to the concentration of the *CPs* in water.
- The ion exchangers and filters remove impurities in proportion to their concentration in the coolant.
- The activity due to originally present impurities (intrinsic activity) is negligible.
- The coupled equations developed in the model are applicable regardless of corrosion pattern, however we have assumed a uniform time dependent corrosion in the coolant circuit and have ignored the space distribution effects.

The time dependent concentration buildup is established by balancing the rate of production of radioactive nuclei and the rate at which they are lost because of different exchange pathways. These exchange pathways include purification of coolant,

Table 1
Corrosion products and their reaction properties (Nasir et al., 2017).

Sr.#	Reaction	Corrosion product	Activation cross section	γ-ray energy
1	^{58}Fe (n, γ) ^{59}Fe (E_n > 11.60 MeV) ^{23}Na (n, γ) ^{24}Na (E_n is thermal)	^{24}Na ($T_{1/2}$ = 15.40 h)	6×10^{-4} b 0.53 b	4.10 MeV (100%)
2	^{58}Fe (n, γ) ^{59}Fe (E_n is thermal)	^{59}Fe ($T_{1/2}$ = 45.10 h)	0.90 b	1.17 MeV (99.99%) 1.33 MeV (99.99%)
3	^{98}Mo (n, γ) ^{99}Mo (E_n > 3.10 MeV)	^{99}Mo ($T_{1/2}$ = 67.00 h)	0.45 b	0.78 MeV (8%) 0.74 MeV (8%)
4	^{59}Co (n, γ) ^{60}Co	^{60}Co ($T_{1/2}$ = 5.30 y)	20.00 b	1.17 MeV (99.99%) 1.33 MeV (99.99%)
5	^{55}Mn (n, γ) ^{56}Mn (E_n is thermal)	^{56}Mn ($T_{1/2}$ = 2.58 h)	13.40 b	2.13 MeV (15%) 1.81 MeV (24%) 0.85 MeV (99%)

deposition of the materials on surfaces, leakage from the system and radioactive decay of activated products. Different pathways leading to these production and loss mechanisms are schematically described in Fig. 1.

The concentration of target nuclides (atoms cm^{-3}) in the primary coolant water, on the inner walls of the piping and on the core surfaces have been denoted by N_w, N_p and N_c respectively. Similarly, the concentrations of the activated nuclides (atoms cm^{-3}) in the primary coolant water, on the inner walls of the piping and on the core surfaces have been denoted by n_w, n_p, and n_c respectively. Then the rate of change of active material concentration in primary coolant is given by Deeba et al. (1999) and Jaeger (1970);

$$\frac{dn_w}{dt} = \sigma\phi_{\in}N_w - \left(\sum_j \frac{\varepsilon_j Q_j}{V_w} + \sum_k \frac{l_k}{V_w} + \lambda\right)n_w + \frac{k_p}{V_w}n_p + \frac{k_c}{V_w}n_c \qquad (1)$$

Here σ is the group constant for the production of isotope from target nuclide; $\phi_{\in}$ is the effective group flux (neutrons/cm^2/s). The sum over j for $\varepsilon_j Q_j$ is given as following:

$$\varepsilon_j Q_j = \varepsilon_i Q_i + \varepsilon_f Q_f + \varepsilon_c Q_c + \varepsilon_p Q_p \qquad (1a)$$

Here the quantities $\varepsilon_i Q_i$, $\varepsilon_f Q_f$ $\varepsilon_c Q_c$ $\varepsilon_p Q_p$ are removal rates (cm^3 s^{-1}) due to ion exchanger, by the filters deposition, on the core surfaces and deposition on pipes respectively. The term l_k is the rate (cm^3 s^{-1}) at which primary coolant loop loses water from its kth leak; k_p and k_c are rates (cm^3 s^{-1}) at which isotopes are removed from the scale on piping and the core respectively. For a typical *PWR* the measured values of these removal rates are given in Table 2. The first term in Eq. (1) represents the production of radioactive isotopes. The second term is the rate at which the active nuclides are lost because of purification by the ion-exchanger and filters, deposition on the piping and core and decay of the activated nuclei. The third and fourth terms are the rates at which activity is re-introduced into the coolant by erosion from the scale present on surface of piping and reactor core. Here $\phi_{\in}$ is effective 10

$$T_c = H\rho A/w(t)\ldots. \qquad (1c)$$

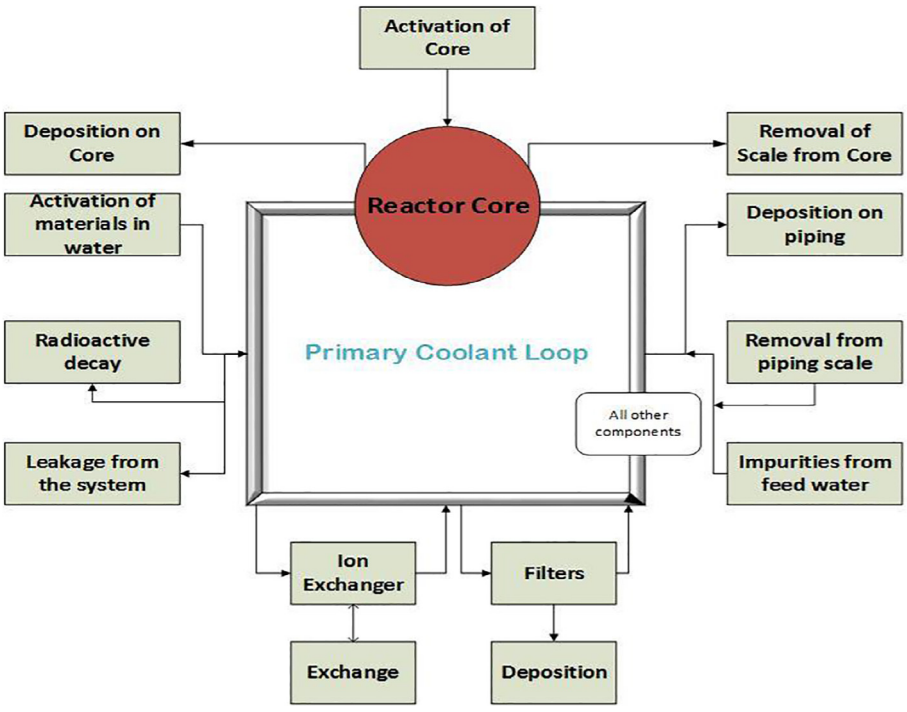

Fig. 1. Schematic of exchange pathways for modeling activation products in primary coolant circuit.

Table 2
Fractional exchange rates of a typical *PWR* (Deeba et al., 1999; Jaeger, 1970).

Rate Description	Value1 and Unit	Value2 and Unit
Deposition on core	$\varepsilon_c Q_c/V_w = 5.835 \times 10^{-5}\ s^{-1}$	$\varepsilon_c Q_c/V_c = 8.81 \times 10^{-6}\ s^{-1}$
Deposition on piping	$\varepsilon_p Q_p/V_w = 1.00 \times 10^{-6}\ s^{-1}$	$\varepsilon_p Q_p/V_c = 1.00 \times 10^{-5}\ s^{-1}$
Ion-exchanger removal ($\varepsilon_I Q_I$)	$\varepsilon_I Q_I/V_w = 5.70 \times 10^{-5}\ s^{-1}$	
Re-solution ratio for core (K_c)	$K_c/V_w = 2.918 \times 10^{-6}\ s^{-1}$	$K_c/V_c = 4.406 \times 10^{-6}\ s^{-1}$
Re-solution ratio for piping (K_p)	$K_p/V_w = 5.0 \times 10^{-7}\ s^{-1}$	$K_p/V_p = 5.0x \times s^{-1}$
Volume of primary coolant	$V_w = 1.37 \times 10^7\ cm^3$	
Volume of scale on core (V_c)	$V_c = 9.08 \times 10^6\ cm^3$	
Average corrosion rate (C_0)	$C_0 = 2.40 \times 10^{-13}\ g\ cm^{-2}\ s^{-1}$	

Here H is core height, ρ is density of coolant at operating temperature and pressure and $w(t)$ is time dependent flow rate. The circulating time of a particle through the primary coolant system is denoted by T_L and for primary loop length L it can be estimated as LT_c/H.

The rate of buildup of target nuclide concentration in coolant water can be written as;

$$\frac{dN_w}{dt} = -\left(\sum_j \frac{\varepsilon_j Q_j}{V_w} + \sum_k \frac{l_k}{V_w} + \sigma\phi_{\in}\right)N_w + \frac{k_p}{V_w}N_p + \frac{k_c}{V_w}N_c + S_w \quad (2)$$

$$S_w = \frac{C_0 S N_0 f_n f_s}{V_w A}\ldots \quad (2a)$$

$$\frac{dn_c}{dt} = \sigma\phi_0 N_c + \frac{\varepsilon_c Q_c}{V_c}n_w - \left(\frac{k_c}{V_c} + \lambda\right)n_c \quad (3)$$

The rate of The C_0 is effective corrosion rate ($gm\ cm^{-2}\ s^{-1}$), S is area of the system exposed to the coolant for corrosion (cm^2), N_0 is Avogadro's number (6.02×1023 atoms $gm^{-1}\ mol^{-1}$), A is Atomic weight of target nuclide ($gm\ mol^{-1}$), fn is natural abundance of target nuclide and fs is abundance of target nuclide in the system. The rate of active nuclides buildup on the cooling system inside the reactor core is given by;

target nuclei buildup on the core scale is given by the following balance;

$$\frac{dN_c}{dt} = \frac{\varepsilon_c Q_c}{V_c}N_w - \left(\frac{k_c}{V_c} + \sigma\phi_0\right)N_c \quad (4)$$

The rate of deposition of active material on the piping scaling can be obtained from the following relation;

$$\frac{dn_p}{dt} = \frac{\varepsilon_p Q_p}{V_p}n_w - \left(\frac{k_p}{V_p} + \lambda\right)n_p \quad (5)$$

Here V_p is the volume of scale on the piping (cm^3).

The rate at which target nuclei buildup on the piping scale is given by the following relation;

$$\frac{dN_p}{dt} = \frac{\varepsilon_p Q_p}{V_p}N_w - \frac{k_p}{V_p}N_p \quad (6)$$

2.1. The power maneuvering based mathematical model

In order to study the dynamic behavior of *CPA* under power maneuvering conditions, the power levels are modeled using following approach. If $p(t)$ is reactor operational power at any time t and p_0 is *Rated Thermal Power (RTP)* of reactor, then any linear variation in reactor power is defined as:

$$p(t) = f(t)p_0$$

The $f(t)$ is a normalized power parameter that can describe various power levels and power transient conditions. The parameter $f(t)$ describes any linear increase or decrease in reactor operational power as following;

$$f(t) = \begin{cases} p_1, & t < t_s \\ p_1 - \mu(t - t_{ts}), & t_{ts} \leqslant t < t_{te} \\ p_2, & t \geqslant t_{te} \end{cases}$$

Here p_1 is percentage *RTP* at which reactor is operating at any time t before the start of transient at time t_{ts}, μ is slope of linear increase or decrease in power during the transient and p_2 is percentage *RTP* at which reactor operates after the end of transient at time t_{te}.

The neutron flux is representative of operating power of reactor, so as the reactor power changes the flux in the reactor core also changes. Therefore, the group flux ϕ_0 averaged over the geometry of core is replaced with $f(t)\phi_0$ and similarly $\phi_{\in}$ with $f(t)\phi_{\in}$ in all of the equations in the above described model. Thus, we get following set of equations.

$$\frac{dn_w}{dt} = \sigma f(t)\phi_{\in}N_w - \left(\sum_j \frac{\varepsilon_j Q_j}{V_w} + \sum_k \frac{l_k}{V_w} + \lambda\right)n_w + \frac{k_p}{V_w}n_p + \frac{k_c}{V_w}n_c \quad (7)$$

$$\frac{dN_w}{dt} = -\left(\sum_j \frac{\varepsilon_j Q_j}{V_w} + \sum_k \frac{l_k}{V_w} + \sigma f(t)\phi_{\in}\right)N_w + \frac{k_p}{V_w}N_p + \frac{k_c}{V_w}N_c + S_w \quad (8)$$

$$\frac{dn_c}{dt} = \sigma f(t)\phi_0 N_c + \frac{\varepsilon_c Q_c}{V_c}n_w - \left(\frac{k_c}{V_c} + \lambda\right)n_c \quad (9)$$

$$\frac{dN_c}{dt} = \frac{\varepsilon_c Q_c}{V_c}N_w - \left(\frac{k_c}{V_c} + \sigma f(t)\phi_0\right)N_c \quad (10)$$

$$\frac{dn_p}{dt} = \frac{\varepsilon_p Q_p}{V_p}n_w - \left(\frac{k_p}{V_p} + \lambda\right)n_p \quad (11)$$

$$\frac{dN_p}{dt} = \frac{\varepsilon_p Q_p}{V_p}N_w - \frac{k_p}{V_p}N_p \quad (12)$$

The above system of coupled differential Eqs. (7)–(12) is suitable to describe the dynamic response of *CPA* during a variety of power maneuvering conditions.

2.2. AP-1000 reactor core configuration and flux calculations

The Westinghouse *AP-1000* has rated core power of 3400 MW_{th}. It has enriched UO_2 as fuel and light water as a coolant and moderator. The reactor core contains a matrix of fuel rods assembled into mechanically identical 157 fuel assemblies along with control and structural elements. The fuel assemblies are arranged in a pattern, which approximates a right circular cylinder. Three radial regions in the core have different enrichments to establish a favorable power distribution. The enrichment of the fuel in the initial core ranges from 2.35% to 4.50%. The core is designed for a fuel

cycle of 18 months with a 93% capacity factor and a region average discharge burnups as high as 60,000 MWd/tU. Light water and stainless steel reflectors surround the core from top, bottom, and in the radial direction. The thickness of the top, bottom, and radial reflector material is approximately 25 cm, 25 cm and 38 cm, respectively (Elsawi and Hraiz, 2015). Table 3 describes typical design specification of *AP-1000* reactor.

Each of the *AP-1000* fuel assemblies consists of a 17 × 17 square lattice array, out of which 264 are fuel rods, 24 are guide tubes for reactor control and one central instrumentation tube. Burnable absorbers, in the form of *Discrete Burnable Absorbers (PYREX)* and *Integrated Fuel Burnable Absorber (IFBA)* rods are used to provide partial control of excess reactivity in the first core. The *PYREX* rods are removed from the core after first cycle. The burnable absorber loading controls peaking factors and prevents the moderator temperature coefficient of the core from becoming positive at normal operating conditions. The *PYREX* and *IFBA* rods are arranged in assemblies in three and five different configurations, respectively, giving rise to total nine distinct assembly types in the *AP-1000* reactor core. Fig. 2 shows the radial enrichment map of reactor core and configuration of fuel assembly for *AP-1000*.

The *MCNP* is a powerful and versatile tool that can be used for calculations of multiplication factor, reaction rates, saturated activities, neutron fluxes and spectra, power peaking factors, reaction rate distributions, shielding etc. Its main advantage is the ability to handle complicated geometries. Using the structural design data in Table 3 and composition of the respective materials (Stefani et al., 2015), the reactor was modeled to calculate neutron flux. The *MCNP* code was used to calculate core averaged group fluxes in the *AP-1000* reactor core. The *MCNP* provides the flux of neutrons through the tally F4; the results are normalized to source

Table 3
Typical design specifications of *AP-1000* reactor (Stefani et al., 2015).

Parameter	Value
Power	
Thermal (MW)	3400
Electrical (net) (MW)	1090
Specific power (kW/kg U)	40.20
Power density (MW/m$^{3)}$	109.70
Thermal (MW)	3400
Electrical (net) (MW)	1090
Specific power (kW/kg U)	40.20
Core	
Height (m)	4.27
Diameter (m)	3.04
Power density (MW/m^3)	109.70
Fuel	
No. of Fuel Assemblies	157
Rod array dimension	17x17
Rods per assembly	264
Rod pitch (mm)	12.60
Transverse dimension of assembly (mm × mm)	214 × 214
Fuel loading, UO_2 (kg)	95,974
Material	UO_2
Pellet diameter (mm)	8.1915
Number of fuel rods	41,448
Rod, OD (mm)	9.50
Diameter gap (mm)	0.1651
Clad thickness (mm)	0.5715
Clad material	Zirc. Alloy
Fuel pellet length (mm)	9.83
Mass of UO_2/m (kg/m)	6.54
Enrichment levels	2.35w/o, 3.40w/o, 4.50w/o
Coolant	
Pressure (MPa)	15.51
Inlet temperature (°C)	279.44
Average temperature in core (°C)	303.39
Total thermal design flow rate of vessel (kg/s)	14300.76

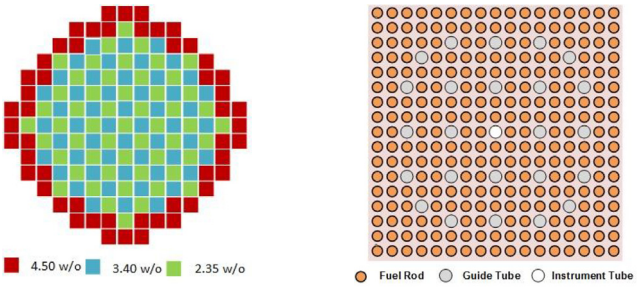

(a) Radial enrichment map **(b)** Fuel assembly configuration

Fig. 2. The radial enrichment map of reactor core and fuel assembly configuration for *AP-1000*.

of neutrons and must be scaled properly for absolute values. The result of F4 tally flux, ϕ_{F4} can be normalized to the desired power using the following equation (Luka Snoj, 2006);

$$\phi_0 = \frac{P(Watt)\bar{\nu}\left(\frac{n}{fission}\right)}{1.6023.10^{-13}\left(\frac{J}{MeV}\right)w_f(MeV/fission)}\phi_{F4} \tag{13}$$

Here P is power, $\bar{\nu}$ is average number of neutrons released by fission, w_f is the energy released per fission and ϕ_{F4} is the flux result given by the tally F4.

3. CPA computing scheme

Based on the above model, a MATLAB computer program *CPA-AP1000*, has been developed in this work. It calculates the *CPA* as a function of reactor operation time under steady state operation and power maneuvering transients. After initialization, it first calculates group fluxes using Tally-4 of the *MCNP* code. Since the *MCNP* results are normalized to one source neutron, the result has to be properly scaled in order to get absolute comparison to the measured quantities of flux. Therefore, the scaling factor is applied in data processing and F4 tally results of core averaged group fluxes are scaled to desired fission neutron source (power) level using Eq. (13). The system of coupled differential equations is solved using fourth order Runge Kutta method. The overall computational scheme is shown in Fig. 3.

4. Results and discussion

The simulations for dynamic response analysis of *CPA* were started at time t = 0, when the reactor was considered to be operating in steady state having no impurities at initial stages. It has been assumed that the system material corrodes uniformly and homogeneously with constant corrosion rate. The experimental values of different factional exchange rates employed in the present analysis are shown in Table 2. The *CPA* is highly sensitive to the ion-exchange removal rates, as observed in the sensitivity analysis of the parameters involved in the under consideration model (Mirza et al., 2010). The ion-exchange removal rate $\varepsilon_I Q_I$ must be higher enough to regard deposition, re-solution and leakage as second-order effects. (Mirza et al., 1998). The optimum removal rate of the coolant activity by the ion exchanger was determined for *AP-1000*, using the same approach as adopted for typical *PWRs*. The specific activity due to ^{24}Na as a function of reactor operation time was calculated for different values of ion exchanger removal rate, using *CPA-AP1000* code. The resulting saturation specific activity of ^{24}Na as a function of different ion exchange removal rate is shown in Fig. 4.

The saturation activity response as a function of ion-exchanger removal rate for *AP-1000* follows the same trend as that for typical

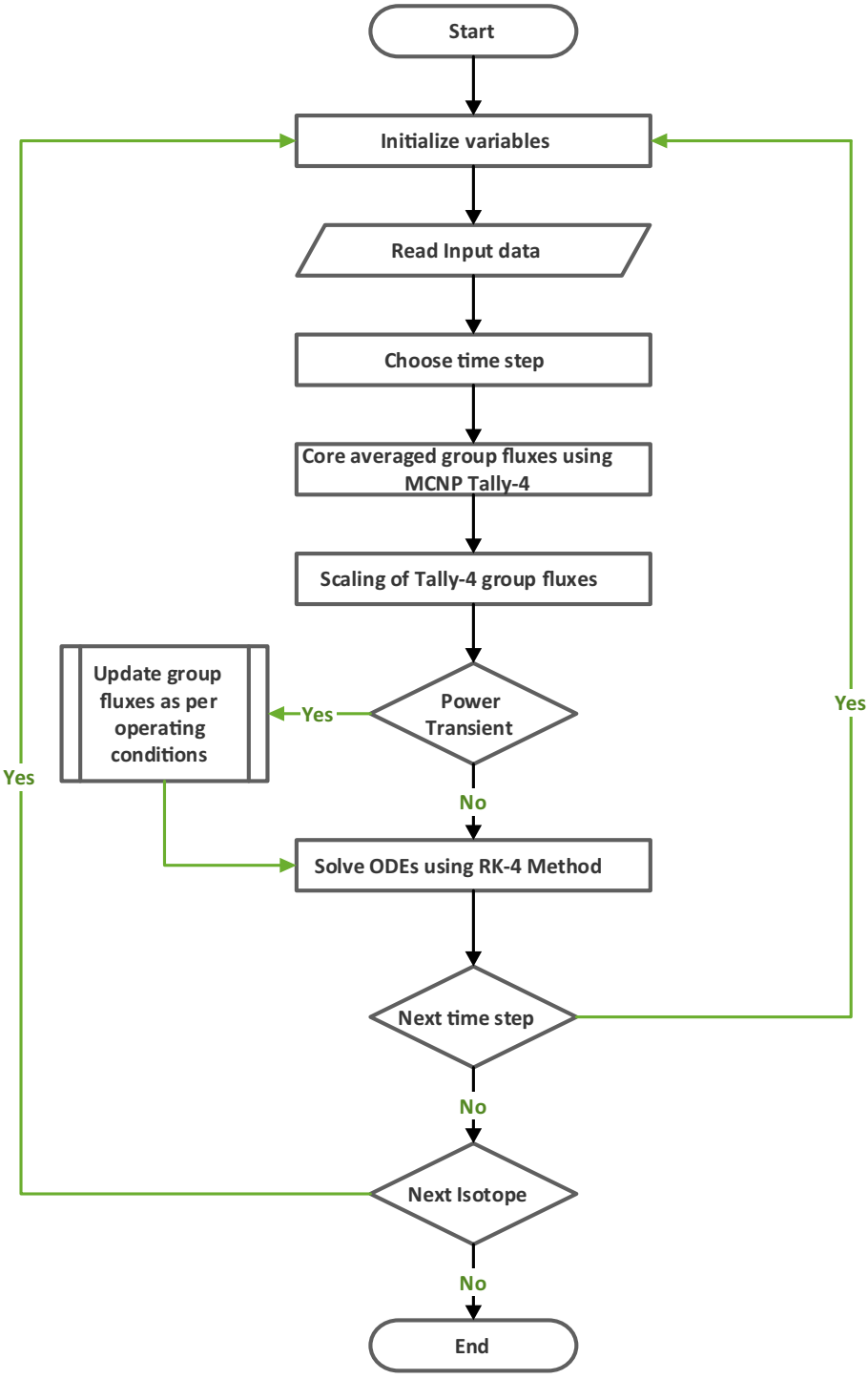

Fig. 3. Flow chart for computing *CPA* of different isotopes under steady state operation and power maneuvering transients.

PWRs. The saturation activity is high when the value of ion exchanger removal rate $\varepsilon_I Q_I$ is low and it decreases in a non-linear fashion as the ion exchanger removal rate is increased. When the value of $\varepsilon_I Q_I$ is increased higher than 400 $cm^3\ s^{-1}$ the saturation activity value varies with a minor slope and becomes almost constant when the value of ion exchange removal rate reaches 600 $cm^3\ s^{-1}$. Therefore, the removal rate of 600 $cm^3\ s^{-1}$ was selected to study dynamic behavior of specific activity due to dominant *CPs* in the present study.

4.1. CPA response under steady state operation

The dominant *CPs* (^{56}Mn, ^{24}Na, ^{59}Fe, ^{60}Co and ^{99}Mo) for a stainless steel based primary coolant structure was considered in this study. The specific activity buildup response of the *CPs* was simulated under steady state operating conditions using *CPA-AP1000* code. In the specific activity buildup response of all *CPs* under study, initially the specific activity concentration increases rapidly as shown in Fig. 5. The initial rapid increase in specific activity is

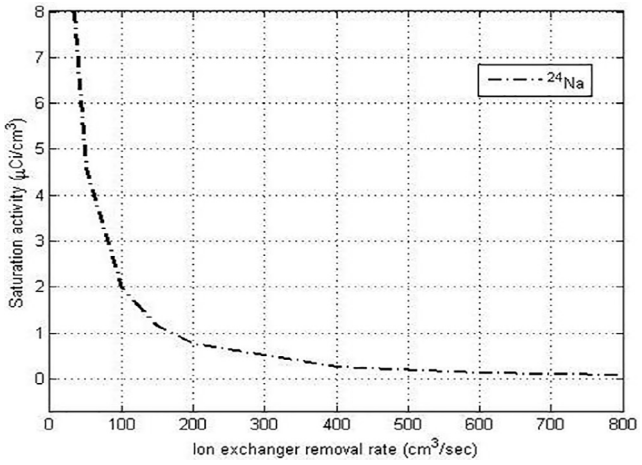

Fig. 4. Saturation specific activity of ^{24}Na at various ion exchanger removal rates for *AP-1000*.

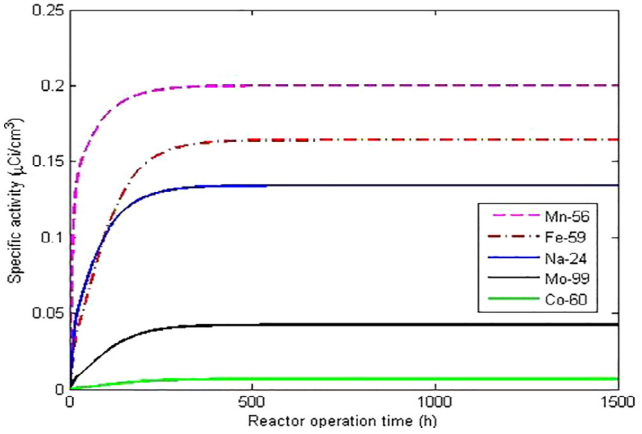

Fig. 5. The specific activity buildup of A*CPs* under steady state full power operation.

due to the fact that initial corrosion rates in a new cooling system is higher than the equilibrium rate (Jaeger, 1970). The initial higher corrosion rate results in a rapid production of target materials at the beginning and hence more *ACPs* during every pass from the reactor core. After passing some time, the *CPs* start accumulating on the coolant channel piping inner walls surfaces and on the core structures. Furthermore, the *CPs* are also removed due to continuous ion exchange operation and the use of filters. A balance between the removal rate and accumulation of the *CPs* on piping and cores surfaces leads to a saturation specific activity value after passing some time.

The ^{56}Mn is the largest contributor to the total specific activity. Its specific activity is about 36.51% of the total specific activity in *AP-1000*. It has saturation value of 0.2000 μCi cm^{-3}. The specific activity response of ^{56}Mn is more rapid as compared to all of the other *ACPs*, it is mainly due to the short half-life as compared to other *CPs* of interest. The ^{56}Mn reaches 90% of it saturation value after 100 h of startup time. The ^{59}Fe increases slowly as compared to ^{24}Na. The contribution of ^{59}Fe and ^{24}Na to the total activity is 29.97% and 24.51% respectively. The ^{59}Fe finally approaches a higher saturation value of 0.1641 μCi cm^{-3} as compared to the saturation value of 0.1342 μCi cm^{-3} for ^{24}Na. The saturation concentrations for ^{59}Fe and ^{24}Na reaches 90% of their values in about 200 h and 165 h respectively. The ^{99}Mo and ^{60}Co have longer half-lives as compared to other *CPs* under study and they contribute less towards the total specific activity during reactor operation. The contribution of ^{99}Mo and ^{60}Co to the total specific activity is 7.76% and 1.24% respectively. The saturation activities of ^{99}Mo and ^{60}Co are 0.0425 μCi cm^{-3} and 0.0068 μCi cm^{-3}. The ^{99}Mo and ^{60}Co reaches 90% of their values in about 216 h and 280 h respectively.

4.2. Comparison of CPA in AP-1000 and a typical PWR

The *CPA* behavior of dominant *CPs* in a typical *PWR*, having the same thermal power as that of Westinghouse *AP-1000*, has already been analyzed using *CPAIR-P* code (Deeba et al., 1999). The behavior of *ACPs* in *AP-1000* is simulated using *CPA-AP1000* under the same operating conditions as that for *PWR* considered in *CPAIR-P* code. The coolant specific activity curves due to *ACPs* in primary loop *AP-1000* and a typical *PWR* are compared in Fig. 6. The buildup curves of corresponding *ACPs* in *AP-1000* and typical *PWR* has been observed to follow similar trends. The respective *ACPs* in *AP-1000* are noticed to ultimately acquire lower saturation values as compared to the typical *PWR* under consideration.

The expected difference in corresponding buildup curves for *AP-1000* and the *PWR* is mainly due to change in design specifications for reactor core and primary circuit of both reactors. The amendment in neutron flux calculation tools in codes used for typical *PWR* and *AP-1000* is also a factor responsible for the difference observed. The CPAIR-P uses LEOPARD and ODMUG codes for energy dependent neutron flux calculations in a typical *PWR* core, whereas, *MCNP* serves the same purpose in *CPA-AP-1000.* The LEOPARD calculates group constants and ODMUG calculates ultimate energy dependent group fluxes. The MCNP has removed the need of combining typical two-step procedure required for neutronics calculations in deterministic codes. The MCNP is a modern Monte Carlo based code, having ability to accurately model the complex geometries. The calculations executed by MCNP are more reliable because it treats individual particles for the related calculations and uses updated cross section libraries for accurate calculations. The comparison of results computed by *CPA-AP1000* and CPAIR-P under a particular power and set of operating conditions have shown good agreement. This exhibits that *CPA-AP1000* owns reasonable computational reliability.

4.3. CPA response under power maneuvering conditions

The *MSHIM* bank scheme has distinct advantage of providing both positive and negative reactivity insertion capability in the event of an operational transient. Insertion of positive and negative reactivity in the reactor core can ultimately lead to power transients during load changes. The *MSHIM* core control strategy enables the *AP-1000* reactor to respond the following load change transients (Westinghouse Electric Company, 2005):

(1) Daily load follow operations
(2) Step load changes of plus or minus 10%
(3) Ramp load increases and decreases of 5% per minute

In subsequent investigations, MSHIM based power maneuvering transients are incorporated at the time when *CPA* have already gained saturation value. The pre-transient saturated value of *CPA* is a base value to compare influence induced by MSHIM based power transients on *CPA*. The parametric study given in following sections provide a variety of analyses to quantify the effect of different design based power transients on *CPA*.

4.3.1. CPA behavior under MSHIM based load follow transients

The *MSHIM* control based, load follow transients are incorporated in the system at *Middle of Cycle (MOC)*, after 750 h of steady

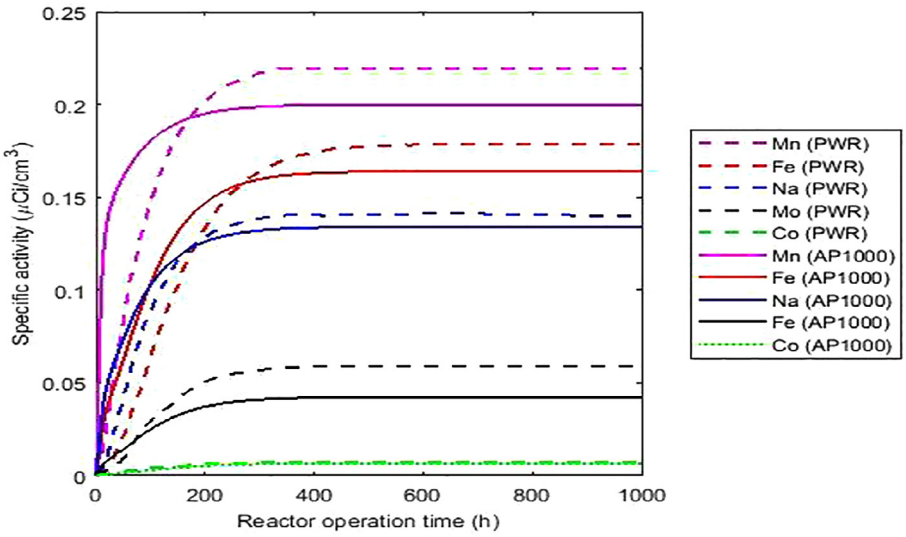

Fig. 6. The primary coolant specific activity buildup curves due to *ACPs* in *AP-1000* and a typical *PWR*.

state full power operation of the reactor. The following possible load follow patterns were incorporated as transients at *MOC*.

- 100-90-100%, 3-6-3 h load follow pattern in which the power varies from 100% to 90% in 3 h, holds at 90% for 6 h, and then rises to 100% in 3 h.
- 100-75-98%, 3-6-3 h load follow pattern in which the power varies from 100% to 75% in 3 h, holds at 75% for 6 h, and then rises to 98% in 3 h.
- 100-50-83%, 3-6-3 h load follow pattern in which the power varies from 100% to 50% in 3 h, holds at 83% for 6 h, and then rises to 100% in 3 h.

The representative change in neutron flux under above described load follow patterns is shown in Fig. 7. The flux mainly follows the same trend as that of power, it increases and decreases with increase and decrease in power level. If power is constant, then correspondingly flux also maintains its constant value. The variation in neutron flux values can ultimately effect the *CPA* levels during reactor operation.

The simulations were done to analyze the *CPA* behavior under load follow transients and the specific activity behavior of ^{56}Mn for various load follow power maneuvering transients is shown in Fig. 8. For all of the transients, during the period (750–753) of decreasing power transient, the specific activity value decreases rapidly depending on the rate of power decrease. If power decrease rate is more rapid, the specific activity falls more rapidly and vice versa. For various levels of operating power during constant power operation period (753–759), the specific activity decrease rate retains its previous trend of decrement rate same as prior to the constant operating power. For the period (759–762) of increasing power transient, the specific activity value start increasing rapidly for different operating power levels depending on various rates of power increment. If power increment rate is rapid, specific activity rises more rapidly and vice versa. The *CPA* behavior of ^{56}Mn during load follow transients showed direct dependence on the power maneuvering level at different instances of time. In all cases of load follow transients, the specific activity of ^{56}Mn settled to a new saturation value after the end of various load follow transients. For anticipated load follow transients, the post saturation specific activity value showed direct relation with net change in power before and after the transients. The higher the difference between pre-transient and post-transient power levels, the longer it takes to achieve saturation value and vice versa. Therefore, the rate of specific activity decrement during various constant power operation periods mainly depend on rate of power decrement, prior to constant operational power period.

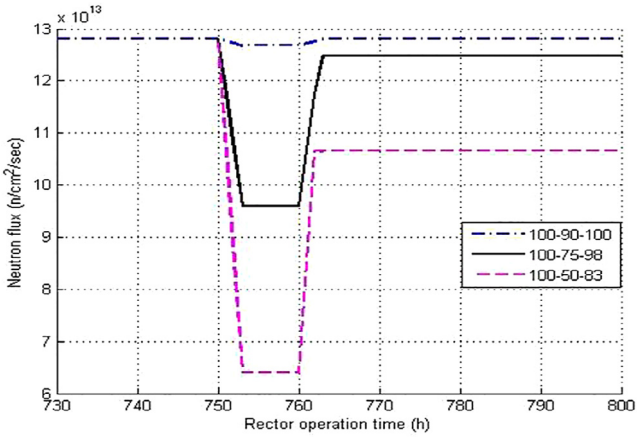

Fig. 7. The representative neutron flux changes in *AP-1000* under load follow transients.

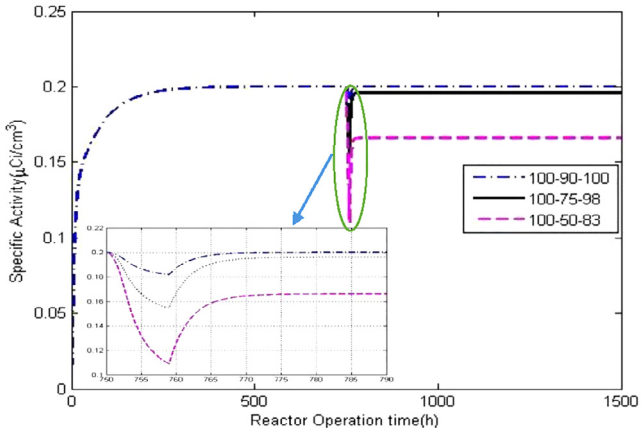

Fig. 8. Specific activity of ^{56}Mn under load follow transients.

4.3.2. CPA behavior during MSHIM based step load transients

The *MSHIM* rod control system can accommodate a step power swing as large as 10% of *RTP*. Such step changes in load demand can result from disturbances in the electrical network to which the unit is tied. The reactor control system is designed to restore plant equilibrium without reactor trip following a 10% step change in turbine load demand initiated from nuclear plant equilibrium conditions between 15 and 100% of full load (the power range for automatic reactor control) (Westinghouse Electric Company, 2005). To analyze the *CPA* behavior, during the step load power maneuvering, following power increasing step load transients incorporating power increment as 3% of *RTP*, 7% of *RTP* and 10% of *RTP* are incorporated. The change in neutron flux duet to such step load changes is shown in Fig. 9.

The simulations were done to analyze the behavior of *CPA* under the above described transients. The transients are induced at the MOC and reactor is considered to be operating in steady state before and after the transient. The reactor power before the occurrence of increasing step load transients is considered to be 90% of RTP before occurrence of transients. The specific activity of ^{56}Mn has been simulated to investigate the effect of above described step load transients. The specific activity behavior of the ^{56}Mn under above described such transients is shown in Fig. 10. The value of specific activity increases sharply as step load increments occur. It has been observed that the specific activity increase is sharper for a larger step of power increment as compared to the shorter power increment steps. However, after some time, the specific activity increase rate becomes slower and finally saturates. The post transient saturation value mainly depends on net power difference before and after the transient. The more the net power difference between pre-transient and post-transient power more later the post transient saturation value is achieved and vice versa.

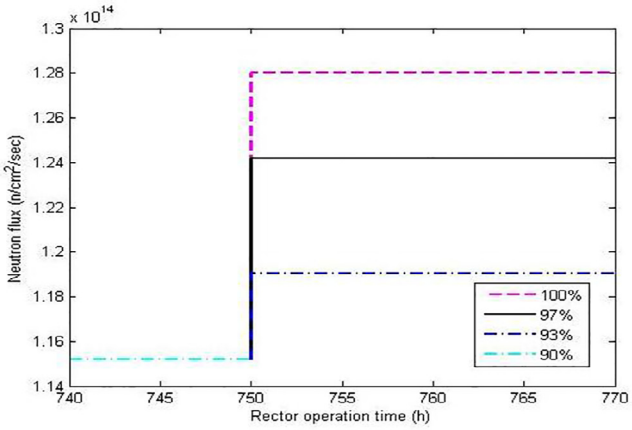

Fig. 9. Change in neutron flux under various step load transients.

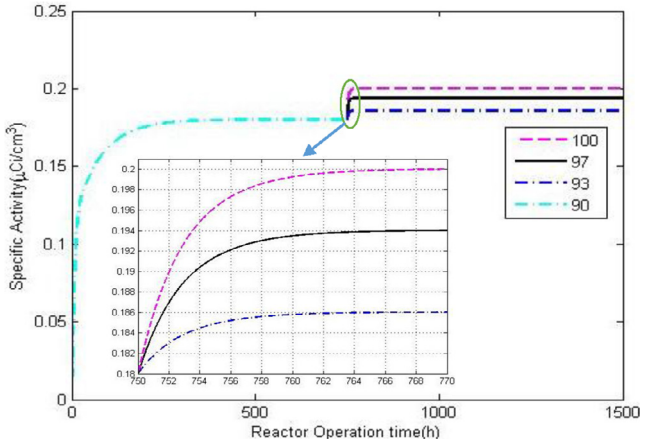

Fig. 10. Specific activity of ^{56}Mn during different step load transients.

4.3.3. Ramp load regulation and scram transients

Frequent load swings may occur during any given day of plant operation. *MSHIM* control system is feasible to accommodate up to five-percent per minute power ramp rates that can occur in rapid succession during load regulation operations of nuclear power stations (Wang et al., 2014). The load regulation operation is analogous to load follow operation, only difference is that it is on smaller and more rapid scale. To study the *CPA* behavior due to ^{56}Mn for such excessive load regulation incidents, different cases of load regulation are considered as following:

- The demand load of the reactor is decreased from 100% *RTP* to 90% *RTP* at a rate of 2% per minute.
- The demand load of the reactor is decreased from 100% *RTP* to 85% *RTP* at a rate of 3.5% per minute.
- The demand load of the reactor is decreased from 100% *RTP* to 80% *RTP* at a rate of 5% per minute.

The change in neutron flux under above described load regulation transients is shown in Fig. 11.

The analyses have been further extended to analyze the behavior of specific activity caused by ^{56}Mn, under scram transients. The resultant specific activity under above described load regulation is simulated accordingly. The analyses are further extended to investigate the effect of various scram transients. The results of specific activity of coolant due to ^{56}Mn is exhibited in Fig. 12.

In all of the load regulation cases, specific activity decrease rate has shown dependence on power decrease rate during load regulation incidents. However, new saturation value is attained depending on the net change in reactor operational power before and after the load regulation. The more the difference between the power before and after the transient the later saturation value is achieved and vice versa. In all of the postulated scram transients, it is evident that the specific activity due to ^{56}Mn suddenly decreased after the scram transients. The sudden decrease in ^{56}Mn activity after the scram is mainly due to its short half-life and further production of this activated product was discontinued due to strike of neutron production in the reactor core.

The preceding sections have presented effect of design based power maneuvering transients on *CPA* in primary coolant of *AP-1000*. The similar effects on coolant activity during power transient

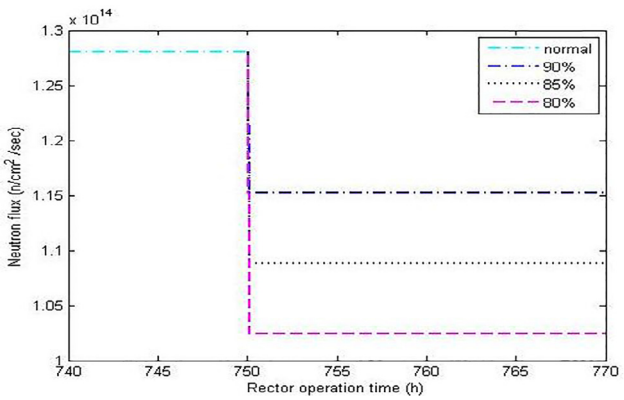

Fig. 11. Change in neutron flux under various load regulation patterns.

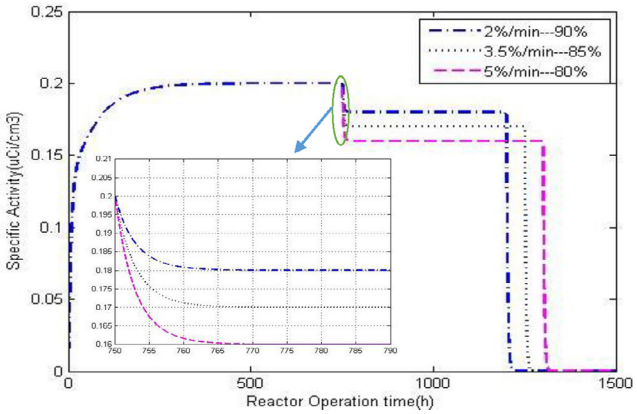

Fig. 12. The specific activity of ^{56}Mn during various load regulation and reactor scram transients.

scenarios have also been witnessed at Turkey Point and Rancho Seco power plants (Mandler et al., 1981), during coolant activity measurement experiments. The *AP-1000* is a fresh design of nuclear reactors fleet. The locally developed code, *CPA-AP1000*, is helpful to foresee associated problems of *CPA* in an innovative reactor, under design based power transients. The computational values worked out by *CPA-AP1000* are reasonably reliable, as comparison of results computed by *CPA-AP1000* and CPAIR-P under a particular power and set of operating conditions (Section 4.2) have shown good agreement.

5. Conclusion

The work carried out in this paper the dynamic analysis of *CPA* in *AP-1000* during steady state operation and *MSHIM* based power-maneuvering transients. A MATLAB program, based on the kinetic model of *CPA* in primary circuit of *AP-1000* has been developed. The program uses *MCNP* code as a subroutine to model the core and finally calculates the neutron flux at different energies. The investigations provide a base for the estimation of radiation dose (γ-field) due to different *ACPs*, which is a major radiation source at operational reactors. The investigations are helpful in making accessibility decisions for on-power inspection and maintenance during small-scale leakage in primary circuit, during steady state operation and power maneuvering transients as well.

The impact of *CPA* in primary coolant for five dominant radionuclides products have been computed numerically. The ^{56}Mn is the largest contributor having specific activity 0.2000 μCi cm^{-3} followed by ^{59}Fe, ^{24}Na, ^{99}Mo and ^{60}Co having specific activity 0.1641 μCi cm^{-3}, 0.01342 μCi cm^{-3}, 0.0425 μCi cm^{-3} and 0.0068 μCi cm^{-3} respectively. The parametric study has been carried out to analyze the *CPA* behavior during various power transients. The *CPA* variation during daily load follow and load regulation transients is observed to have direct dependence on the power-maneuvering rate. However, if decreasing power maneuvering was followed by a steady state power level the specific activity retained its prior pattern of decrease and finally attains a new reduced constant value. For the step load transients, the specific activity value is observed to increase sharply and finally saturated to a new level. During power maneuvering transients, the specific activity was observed to attain a new saturation value depending on the net change in pre-transient and post-transient power levels. The higher the difference between pre-transient and post-transient power levels, the longer it takes to achieve saturation value and vice versa. The specific activity of ^{56}Mn is observed to decrease suddenly after the scram, mainly due to its short half-life and discontinuation in further production. This analysis is helpful in predicting decay behavior of γ-radiation emitted by the short-lived *ACPs* during accessibility of primary circuit after the scram transients.

The *CPA-AP1000* is helpful to foresee associated problems of CPA in a fresh direct design with reasonable computational reliability. The previous studies of *CPA* behavior in *RCS* of *AP-1000* using CAT1.0 code and current development of *CPA-AP1000* have established a base for further research for *AP-1000*, in this field. The work can be extended to analyze *CPA* buildup behavior under more operational parameters and anticipated transients; in addition to power maneuvering transients. Furthermore, the accidental scenarios can also be incorporated in the current model to analyze *CPA* behavior under the worst operational scenarios.

Acknowledgements

The present work has been supported by the China Scholarship Council (CSC) Grant No. 2016GXZO22 and the funding support of National Science & Technology; Major Project of the Ministry of Science & Technology of China (via contract no. 2011ZX06002001). The author gratefully acknowledges the valued discussions with Dr. Muhammad Rafique from AJKU Pakistan during this work. The authors also wish to thank the fellows of School of Nuclear Science and Technology, Xi'an Jiaotong University for providing the necessary help.

References

Comley, G.C.W., 1985. The significance of corrosion products in water reactor coolant circuits. Prog. Nucl. Energy 16, 41–72. https://doi.org/10.1016/0149-1970(85)90005-8.

Deeba, F., Mirza, A.M., Mirza, N.M., 1999. Modeling and simulation of corrosion product activity in pressurized water reactors under power perturbations. Ann. Nucl. Energy 26, 561–578. https://doi.org/10.1016/S0306-4549(98)00087-5.

Elsawi, M.A., Bin Hraiz, A.S., 2015. Benchmarking of the WIMS9/PARCS/TRACE code system for neutronic calculations of the Westinghouse AP1000^{TM} reactor. Nucl. Eng. Des. 293, 249–257. https://doi.org/10.1016/j.nucengdes.2015.08.008.

Génin, J.-B., Brissonneau, L., Gilardi, T., 2016. OSCAR-Na: a new code for simulating corrosion product contamination in SFR. Metall. Mater. Trans. E 3, 291–298. https://doi.org/10.1007/s40553-016-0094-9.

IAEA, 2012. Modelling of transport of radioactive substances in the primary circuit of water-cooled reactors. IAEA-TECDOC-1672, Viana, Austria.

IAEA, 2015. Nuclear power reactors in the world, Reference Data Series No. 2. International Atomic Energy Commission, IAEA-RDS-2/230, Viana, Austria.

Jaeger, R.G., 1970. Engineering Compendium on Radiation Shielding. Springer-Verlag, New York.

Jia, J., 2016. Research on Modeling the corrosion, activity and transport proceeds in PWR primary circuits (MS thesis, May). Xi'an Jiaotong University, Xi'an, China.

Li, L., Zhang, J., He, S., Fu, Y., Chen, Y., 2017b. The development of two-phase three-node model used to simulate the transport of ACPs. Prog. Nucl. Energy 97, 99–105. https://doi.org/10.1016/j.pnucene.2016.12.015.

Li, L., Zhang, J., Guo, Q., Zhang, X., Liu, S., Chen, Y., 2017a. Evaluation of ACPs in China fusion engineering test reactor using CATE 2.1 Code. Sci. Technol. Nucl. Install. https://doi.org/10.1155/2017/2936069.

Lister, D.H., 1984. Corrosion-Products release in Light Water Reactors. EPRI Report NP-3460, Ontario, Canada.

Luka Snoj, M.R., 2006. Calculation of power density with Mcnp in triga reactor. Nucl. Energy New Europe, 1–6.

Mandler, P.J.W., Stalker, A.C., Croney, S.T., Mcisaac, C.V, Soli, G.A., Hartwell, J.K., Eg, L. S.L., 1981. In-Plant Source Term Measurements at Four PWRs, NUREG/CR-1992. USNRC Washington D.C.

Mirza, N.M., Mirza, S.M., Iqbal, M.J., 2011. Recent trends in mathematical modeling and simulation of fission product transport from fuel to primary coolant of PWRs. In: Nuclear Power – System Simulations and Operation. https://doi.org/10.5772/17670.

Mirza, A.M., Mirza, N.M., Mir, I., 1998. Simulation of corrosion product activity in pressurized water reactors under flow rate transients. Ann. Nucl. Energy 25, 331–345. https://doi.org/10.1016/S0306-4549(97)00062-5.

Mirza, S.M., Ra, M., Ahmad, F., Mirza, N.M., 2010. Static and dynamic sensitivity analysis of corrosion product activity in primary coolant circuits of pressurized water reactors. Prog. Nucl. Energy 52, 648–654. https://doi.org/10.1016/j.pnucene.2010.04.001.

Mirza, N.M., Rafique, M., Mirza, S.M., Hyder, M.J., 2005. Simulation of corrosion product activity for nonlinearly rising corrosion on inner surfaces of primary coolant pipes of a typical PWR under flow rate transients. Appl. Radiat. Isotopes 62, 681–692. https://doi.org/10.1016/j.apradiso.2004.12.005.

Nasir, R., Mirza, S.M., Mirza, N.M., 2017. Evaluation of corrosion product activity in a typical PWR with extended cycles and flow rate perturbations. World J. Nucl. Sci. Technol. 7, 24–34. https://doi.org/10.4236/wjnst.2017.71003.

Odano, N., Ishida, T., 2000. Evaluation of buildup of activated corrosion products for highly compact marine reactor DRX without primary coolant water purification system. J. Nucl. Sci. Technol. 37, 584–588. https://doi.org/10.1080/00223131.2000.10874955.

Onoue, M., Kawanishi, T., 2003. Application of MSHIM core control strategy for westinghouse AP1000 nuclear power plant. In: GENES4/ANP2003, Sep 15–19. Kyoto, JAPAN.

Rafique, M., Mirza, N.M., Mirza, S.M., 2003. Computational modeling of accelerating corrosion in primary coolants of a typical PWR. In: Proc. – INMIC, IEEE 7th Int Multi Top. Conf. pp. 482–489. doi: 10.1109/INMIC.2003.1416775.

Rafique, M., Mirza, N.M., Mirza, S.M., Iqbal, M.J., 2010. Review of computer codes for modeling corrosion product transport and activity build-up in light water reactors 55, 263–269.

Seo, M.J., Shim, H.S., Kim, K.M., Hong, S.I., Hur, D.H., 2015. Influence of surface roughness on the corrosion behavior of Alloy 690TT in PWR primary water. Nucl. Eng. Des. 280, 62–68. https://doi.org/10.1016/j.nucengdes.2014.08.023.

Shuran, M., 2016. Modelling of materials corrosion inside RCS based on mixed-conduction model. In: Proceedings of ISSNP 2016 8th International Symposium on Symbiotic Nuclear Power Systems for 21st Century September 26–28 Chengdu, China.

Song, M.C., Lee, K.J., 2003. The evaluation of radioactive corrosion product at PWR as change of primary coolant chemistry for long-term fuel cycle. Ann. Nucl. Energy 30, 1231–1246. https://doi.org/10.1016/S0306-4549(03)00054-9.

Soukieh, M., Jamal, M.H., Ghazi, N., 2012. Mathematical modeling and measurement of the activated corrosion products in the MNSR research reactor. Ann. Nucl. Energy 42, 43–46. https://doi.org/10.1016/j.anucene.2011.09.022.

Stefani, G.L., Rossi, P.R., Maiorino, J.R., Santos, T.A., 2015. Neutronic and Thermal-Hydraulic Calculations for the AP-1000 NPP With the MCNP6 and Serpent Codes. In: 2015 International Nuclear Atlantic Conference – INAC. SP, Brazil.

Sutharshan, B., Mutyala, M., Vijuk, R.P., Mishra, A., 2011. The AP1000 reactor: passive safety and modular design. Energy Proc. 7, 293–302. https://doi.org/10.1016/j.egypro.2011.06.038.

Wang, P., Wan, J., Chen, Z., Sun, J., Zhang, R., He, Z., Zhao, F., 2014. Dynamic simulation and study of Mechanical Shim (MSHIM) core control strategy for AP1000 reactor. Ann. Nucl. Energy 72, 49–62. https://doi.org/10.1016/j.anucene.2014.04.023.

Westinghouse Electric Company, 2005. AP1000 Design Control Document Rev. 15 (Chapter 7).

Zhang, J., Li, L., He, S., Song, W., Fu, Y., Zhang, B., Chen, Y., 2015. Development of a three-zone transport model for activated corrosion products analysis of Tokamak Cooling Water System. Fusion Eng. Des. 111, 407–410. https://doi.org/10.1016/j.fusengdes.2016.02.091.

Zhu, Y., Free, M.L., Woollam, R., Durnie, W., 2017. A review of surfactants as corrosion inhibitors and associated modeling. Prog. Mater. Sci. 90, 159–223. https://doi.org/10.1016/j.pmatsci.2017.07.006.